

CSI: Novelty Detection via Contrastive Learning on Distributionally Shifted Instances

Jihoon Tack^{*†}, Sangwoo Mo^{*‡}, Jongheon Jeong[‡], Jinwoo Shin^{†‡}

[†]KAIST AI [‡]KAIST EE

{jihoontack,swmo,jongheonj,jinwoos}@kaist.ac.kr

Abstract

Novelty detection, *i.e.*, identifying whether a given sample is drawn from outside the training distribution, is essential for reliable machine learning. To this end, there have been many attempts at learning a representation well-suited for novelty detection and designing a score based on such representation. In this paper, we propose a simple, yet effective method named *contrasting shifted instances* (CSI), inspired by the recent success on contrastive learning of visual representations. Specifically, in addition to contrasting a given sample with other instances as in conventional contrastive learning methods, our training scheme contrasts the sample with distributionally-shifted augmentations of itself. Based on this, we propose a new detection score that is specific to the proposed training scheme. Our experiments demonstrate the superiority of our method under various novelty detection scenarios, including unlabeled one-class, unlabeled multi-class and labeled multi-class settings, with various image benchmark datasets.

1 Introduction

Out-of-distribution (OOD) detection [27], also referred to as a novelty- or anomaly detection is the task of identifying whether a test input is drawn far from the training distribution (in-distribution) or not. In general, the OOD detection problem aims to detect OOD samples where a detector is allowed to access only to training data. The space of OOD samples is typically huge (compared to that of in-distribution), *i.e.*, an OOD sample can vary significantly and arbitrarily from the given training distribution. Hence, assuming specific prior knowledge, *e.g.*, external data representing some specific OODs, may introduce a bias to the detector. The OOD detection is a classic yet essential problem in machine learning, with a broad range of applications, including medical diagnosis [3], fraud detection [49], and autonomous driving [13].

A long line of literature has thus been proposed, including density based [66, 43, 7, 12, 52, 57, 17], reconstruction based [55, 68, 50, 48, 8], one-class classifier [56, 53, 54], and self-supervised [15, 26, 1] approaches. Overall, a majority of recent literature is concerned with (a) modeling the representation for a given sample to better encode normality [24, 26], and (b) defining a new detection score [53, 1]. For example, recent studies have shown that inductive biases from neural networks significantly help to learn discriminative features for OOD detection [53, 26].

Meanwhile, recent progress on unsupervised representation learning has proven the effectiveness of *contrastive learning* in various domains, *e.g.*, computer vision [22, 60, 21, 5], audio processing [46], and reinforcement learning [58]. More specifically, contrastive learning extracts a strong inductive bias from data by pulling similar samples yet pushing the others. *Instance discrimination* [62] is a special type of contrastive learning that have achieved state-of-the-art results [21, 5], which only pulls the same instances up to different augmentations.

^{*}equal contribution

Inspired by the recent success of instance discrimination, we aim to utilize its power of representation learning for OOD detection. To this end, we investigate the following questions: (a) how to learn a (more) discriminative representation for detecting OODs and (b) how to design a score function utilizing the representation from (a). We remark that the desired representation for OOD detection may differ from that for standard representation learning [24, 26], as the former aims to discriminate in-distribution and OOD samples, while the latter aims to discriminate *within* in-distribution samples.

We first found that an existing contrastive learning scheme of visual representation is already reasonably effective for detecting OOD samples with an appropriate detection score. We further observe that one can improve its performance by utilizing “hard” augmentations, *e.g.*, rotation, that were known to be harmful and unused for the standard contrastive learning [5]. In particular, while the existing contrastive learning schemes act by pulling all augmented samples toward the original sample, we suggest to additionally push the samples with hard or distribution-shifting augmentations away from the original. We observe that contrasting shifted samples help OOD detection,¹ as the model now learns a new task of discriminating *between* in- and out-of-distribution, in addition to the original task of discriminating *within* in-distribution.

Contribution. We propose a simple yet effective method for OOD detection, coined *contrasting shifted instances* (CSI). Built upon the existing contrastive learning scheme [5], we propose two novel additional components: (a) a new training method which contrasts distributionally-shifted augmentations (of the given sample) in addition to other instances, and (b) a score function which utilizes both the contrastively learned representation and our new training scheme in (a). Finally, we show that CSI enjoys broader usage by applying it to improve the confidence-calibration of the classifiers: it relaxes the overconfidence issue in their predictions for both in- and out-of-distribution samples while maintaining the classification accuracy.

We verify the effectiveness of CSI under various environments of detecting OOD, including unlabeled one-class, unlabeled multi-class, and labeled multi-class settings. To our best knowledge, we are the first to demonstrate all three settings under a single framework. Overall, CSI outperforms the baseline methods for all tested datasets. In particular, CSI achieves new state-of-the-art results² on one-class classification, *e.g.*, it improves the mean area under the receiver operating characteristics (AUROC) from 90.1% to 94.3% (+4.2%) for CIFAR-10 [33], 79.8% to 89.6% (+9.8%) for CIFAR-100 [33], and 85.7% to 91.6% (+5.9%) for ImageNet-30 [26] one-class datasets, respectively. We remark that CSI gives a larger improvement in harder (or near-distribution) OOD samples. To verify this, we also release new benchmark datasets: fixed version of the resized LSUN and ImageNet [38].

We remark that learning representation to discriminate between in- and out-of-distributions is an important but under-explored problem. We think that our work would guide new interesting directions in the future, for both representation learning and OOD detection.

2 CSI: Contrasting shifted instances

For a given dataset $\{x_m\}_{m=1}^M$ sampled from a data distribution $p_{\text{data}}(x)$ on the data space \mathcal{X} , the goal of out-of-distribution (OOD) detection is to model a detector from $\{x_m\}$ that identifies whether x is sampled from the data generating distribution (or in-distribution) $p_{\text{data}}(x)$ or not. As modeling $p_{\text{data}}(x)$ directly is prohibitive in most cases, many existing methods for OOD detection define a *score function* $s(x)$ that a high value heuristically represents that x is from in-distribution.

In Section 2.1, we first briefly review the preliminaries on contrastive learning. Then, we describe two components of our method, *contrasting shifted instances* (CSI): the training scheme and the corresponding score function, in Section 2.2 and Section 2.3, respectively. Finally, we propose an extension of CSI for training *confidence-calibrated* classifiers in Section 2.4.

¹It may not help (in-distribution) classification (see Section 3.2).

²We do not compare with the methods using *external* OOD samples [25, 54].

2.1 Contrastive learning

The idea of *contrastive learning* is to learn an encoder f_θ to extract the necessary information to distinguish similar samples from the others. Let x be a query, $\{x_+\}$, and $\{x_-\}$ be a set of positive and negative samples, respectively, and $\text{sim}(z, z') := z \cdot z' / \|z\| \|z'\|$ be the cosine similarity. Then, the primitive form of the *contrastive loss* is defined as follows:

$$\mathcal{L}_{\text{con}}(x, \{x_+\}, \{x_-\}) := -\frac{1}{|\{x_+\}|} \log \frac{\sum_{x' \in \{x_+\}} \exp(\text{sim}(z(x), z(x')) / \tau)}{\sum_{x' \in \{x_+\} \cup \{x_-\}} \exp(\text{sim}(z(x), z(x')) / \tau)}, \quad (1)$$

where $|\{x_+\}|$ denotes the cardinality of the set $\{x_+\}$, $z(x)$ denotes the output feature of the contrastive layer, and τ denotes a temperature hyper-parameter. One can define the contrastive feature $z(x)$ directly from the encoder f_θ , *i.e.*, $z(x) = f_\theta(x)$ [21], or apply an additional projection layer g_ϕ , *i.e.*, $z(x) = g_\phi(f_\theta(x))$ [5]. We use the projection layer following the recent studies [5, 6].

In this paper, we specifically consider the simple contrastive learning (*SimCLR*) [5], a simple and effective objective based on the task of *instance discrimination* [62]: Let $\tilde{x}_i^{(1)}$ and $\tilde{x}_i^{(2)}$ be two independent augmentations of x_i from a pre-defined family \mathcal{T} , namely, $\tilde{x}_i^{(1)} := T_1(x_i)$ and $\tilde{x}_i^{(2)} := T_2(x_i)$, where $T_1, T_2 \sim \mathcal{T}$. Then the SimCLR objective can be defined by the contrastive loss (1) where each $(\tilde{x}_i^{(1)}, \tilde{x}_i^{(2)})$ and $(\tilde{x}_i^{(2)}, \tilde{x}_i^{(1)})$ are considered as query-key pairs while others being negatives. Namely, for a given batch $\mathcal{B} := \{x_i\}_{i=1}^B$, the SimCLR objective is defined as follows:

$$\mathcal{L}_{\text{SimCLR}}(\mathcal{B}) := \frac{1}{2B} \sum_{i=1}^B \mathcal{L}_{\text{con}}(\tilde{x}_i^{(1)}, \tilde{x}_i^{(2)}, \tilde{\mathcal{B}}_{-i}) + \mathcal{L}_{\text{con}}(\tilde{x}_i^{(2)}, \tilde{x}_i^{(1)}, \tilde{\mathcal{B}}_{-i}), \quad (2)$$

where $\tilde{\mathcal{B}} := \{\tilde{x}_i^{(1)}\}_{i=1}^B \cup \{\tilde{x}_i^{(2)}\}_{i=1}^B$ and $\tilde{\mathcal{B}}_{-i} := \{\tilde{x}_j^{(1)}\}_{j \neq i} \cup \{\tilde{x}_j^{(2)}\}_{j \neq i}$.

2.2 Contrastive learning for distribution-shifting transformations

Chen et al. [5] has performed an extensive study on which family of augmentations \mathcal{T} leads to a better representation when used in SimCLR, *i.e.*, which transformations should f_θ consider as positives. Overall, the authors report that some of the examined augmentations (*e.g.*, rotation), sometimes degrades the discriminative performance of SimCLR. One of our key findings is that such augmentations can be useful for OOD detection by considering them as *negatives* - contrast from the original sample. In this paper, we explore which family of augmentations \mathcal{S} , which we call *distribution-shifting transformations*, or simply *shifting transformations*, would lead to better representation in terms of OOD detection when used as negatives in SimCLR.

Contrasting shifted instances. We consider a set \mathcal{S} consisting of K different (random or deterministic) transformations, including the identity I : namely, we denote $\mathcal{S} := \{S_0 = I, S_1, \dots, S_{K-1}\}$. In contrast to the vanilla SimCLR that considers augmented samples as positive to each other, we attempt to consider them as negative if the augmentation is from \mathcal{S} . For a given batch of samples $\mathcal{B} = \{x_i\}_{i=1}^B$, this can be done simply by augmenting \mathcal{B} via \mathcal{S} before putting it into the SimCLR loss defined in (2): namely, we define *contrasting shifted instances* (con-SI) loss as follows:

$$\mathcal{L}_{\text{con-SI}} := \mathcal{L}_{\text{SimCLR}} \left(\bigcup_{S \in \mathcal{S}} \mathcal{B}_S \right), \quad \text{where } \mathcal{B}_S := \{S(x_i)\}_{i=1}^B. \quad (3)$$

Here, our intuition is to regard each distributionally-shifted sample (*i.e.*, $S \neq I$) as an OOD with respect to the original. In this respect, con-SI attempts to discriminate an in-distribution (*i.e.*, $S = I$) sample from other OOD (*i.e.*, $S \in \{S_1, \dots, S_{K-1}\}$) samples. We further verify the effectiveness of con-SI in our experimental results: although con-SI does not improve representation for standard classification, it does improve OOD detection significantly.

Classifying shifted instances. In addition to contrasting shifted instances, we consider an auxiliary task that predicts which shifting transformation $y^S \in \mathcal{S}$ is applied for a given input x , in order to facilitate f_θ to discriminate each shifted instance. Specifically, we add a linear layer to f_θ for modeling an auxiliary softmax classifier $p_{\text{cls-SI}}(y^S|x)$, as in [15, 26, 1]. Let $\tilde{\mathcal{B}}_S$ be the batch augmented from \mathcal{B}_S via SimCLR; then, we define *classifying shifted instances* (cls-SI) loss as follows:

$$\mathcal{L}_{\text{cls-SI}} := \frac{1}{2B} \frac{1}{K} \sum_{S \in \mathcal{S}} \sum_{\tilde{x}_S \in \tilde{\mathcal{B}}_S} -\log p_{\text{cls-SI}}(y^S = S | \tilde{x}_S). \quad (4)$$

The final loss of our proposed method, *CSI*, is defined by combining the two objectives:

$$\mathcal{L}_{\text{CSI}} = \mathcal{L}_{\text{con-SI}} + \lambda \cdot \mathcal{L}_{\text{cls-SI}} \quad (5)$$

where $\lambda > 0$ is a balancing hyper-parameter. We simply set $\lambda = 1$ for all our experiments.

2.3 Score functions for detecting out-of-distribution

Upon the representation $z(\cdot)$ learned by our proposed training objective, we define several score functions for detecting out-of-distribution; whether a given x is OOD or not. We first propose a detection score that is applicable to any contrastive representation. We then introduce how one could incorporate additional information learned by contrasting (and classifying) shifted instances as in (5).

Detection score for contrastive representation. Overall, we find that two features from SimCLR representations are surprisingly effective for detecting OOD samples: (a) the *cosine similarity* to the nearest training sample in $\{x_m\}$, *i.e.*, $\max_m \text{sim}(z(x_m), z(x))$, and (b) the *norm* of the representation, *i.e.*, $\|z(x)\|$. We discuss the detailed analysis of both features in Appendix H. We simply combine these two features to define a detection score s_{con} for contrastive representation:

$$s_{\text{con}}(x; \{x_m\}) := \max_m \text{sim}(z(x_m), z(x)) \cdot \|z(x)\|. \quad (6)$$

We also discuss how one can reduce the computation and memory cost by choosing a proper subset (*i.e.*, coresets) of training samples in Appendix E.

Utilizing shifting transformations. Given that our proposed \mathcal{L}_{CSI} is used for training, one can further improve the detection score s_{con} significantly by incorporating shifting transformations \mathcal{S} . Here, we propose two additional scores, $s_{\text{con-SI}}$ and $s_{\text{cls-SI}}$, where are corresponded to $\mathcal{L}_{\text{con-SI}}$ (3) and $\mathcal{L}_{\text{cls-SI}}$ (4), respectively.

Firstly, we define $s_{\text{con-SI}}$ by taking an expectation of s_{con} over $S \in \mathcal{S}$:

$$s_{\text{con-SI}}(x; \{x_m\}) := \sum_{S \in \mathcal{S}} \lambda_S^{\text{con}} s_{\text{con}}(S(x); \{S(x_m)\}), \quad (7)$$

where $\lambda_S^{\text{con}} := M / \sum_m s_{\text{con}}(S(x_m); \{S(x_m)\}) = M / \sum_m \|z(S(x_m))\|$ are used as balancing terms since the shifting transformation S can change the feature statistics (See Appendix F for the details).

Secondly, we define $s_{\text{cls-SI}}$ utilizing the auxiliary classifier $p(y^S|x)$ upon f_θ as follows:

$$s_{\text{cls-SI}}(x) := \sum_{S \in \mathcal{S}} \lambda_S^{\text{cls}} W_S f_\theta(S(x)), \quad (8)$$

where $\lambda_S^{\text{cls}} := M / \sum_m [W_S f_\theta(S(x_m))]$ are again balancing terms similarly to above, and W_S is the weight vector in the linear layer of $p(y^S|x)$ per $S \in \mathcal{S}$.

Finally, the combined score for CSI representation is defined as follows:

$$s_{\text{CSI}}(x; \{x_m\}) := s_{\text{con-SI}}(x; \{x_m\}) + s_{\text{cls-SI}}(x). \quad (9)$$

Ensembling over random augmentations. In addition, we find one can further improve each of the proposed scores by ensembling it over random augmentations $T(x)$ where $T \sim \mathcal{T}$. Namely, for instance, the *ensembled CSI* score is defined by $s_{\text{CSI-ens}}(x) := \mathbb{E}_{T \sim \mathcal{T}} [s_{\text{CSI}}(T(x))]$. Unless otherwise noted, we use these ensembled versions of (6) to (9) in our experiments. See Appendix D for details.

Table 1: AUROC (%) values of various OOD detection methods trained on one-class dataset of (a) CIFAR-10, (b) CIFAR-100 (super-class), and (c) ImageNet-30. For CIFAR-10, each column indicates the results of the selected class, and the final column indicates the mean value. For CIFAR-100 and ImageNet-30, we only report the mean AUROC. See Appendix C for additional results. * denotes the values from the reference, and bold denotes the best results.

(a) One-class CIFAR-10												
Method	Network	Plane	Car	Bird	Cat	Deer	Dog	Frog	Horse	Ship	Truck	Mean
OC-SVM* [56]	-	65.6	40.9	65.3	50.1	75.2	51.2	71.8	51.2	67.9	48.5	58.8
DeepSVDD* [53]	LeNet	61.7	65.9	50.8	59.1	60.9	65.7	67.7	67.3	75.9	73.1	64.8
AnoGAN* [55]	DCGAN	67.1	54.7	52.9	54.5	65.1	60.3	58.5	62.5	75.8	66.5	61.8
OCGAN* [48]	OCGAN	75.7	53.1	64.0	62.0	72.3	62.0	72.3	57.5	82.0	55.4	65.7
Geom* [15]	WRN-16-8	74.7	95.7	78.1	72.4	87.8	87.8	83.4	95.5	93.3	91.3	86.0
Rot* [26]	WRN-16-4	71.9	94.5	78.4	70.0	77.2	86.6	81.6	93.7	90.7	88.8	83.3
Rot+Trans* [26]	WRN-16-4	77.5	96.9	87.3	80.9	92.7	90.2	90.9	96.5	95.2	93.3	90.1
GOAD* [1]	WRN-10-4	77.2	96.7	83.3	77.7	87.8	87.8	90.0	96.1	93.8	92.0	88.2
Rot [26]	ResNet-18	78.6	94.3	86.8	81.6	89.9	88.2	88.2	95.1	92.4	90.5	88.6
Rot+Trans [26]	ResNet-18	80.2	96.6	85.9	81.7	91.6	89.8	90.2	96.1	95.1	92.8	90.0
GOAD [1]	ResNet-18	75.5	94.2	82.4	72.1	83.7	84.8	82.8	93.4	92.6	89.8	85.1
CSI (ours)	ResNet-18	90.0	99.1	93.3	86.4	93.8	93.4	95.2	98.6	97.9	95.5	94.3

(b) One-class CIFAR-100 (super-class)			(c) One-class ImageNet-30		
Method	Network	AUROC	Method	Network	AUROC
OC-SVM* [56]	-	63.1	Rot* [26]	ResNet-18	65.3
Geom* [15]	WRN-16-8	78.7	Rot+Trans* [26]	ResNet-18	77.9
Rot [26]	ResNet-18	77.7	Rot+Attn* [26]	ResNet-18	81.6
Rot+Trans [26]	ResNet-18	79.8	Rot+Trans+Attn* [26]	ResNet-18	84.8
GOAD [1]	ResNet-18	74.5	Rot+Trans+Attn+Resize* [26]	ResNet-18	85.7
CSI (ours)	ResNet-18	89.6	CSI (ours)	ResNet-18	91.6

2.4 Extension for training confidence-calibrated classifiers

Furthermore, we show that our proposed method can be extended for training a *confidence-calibrated* classifier [23, 36] from a given labeled dataset $\{(x_m, y_m)\}_m \subseteq \mathcal{X} \times \mathcal{Y}$: Here, the goal is to model a classifier $p(y|x)$ that is (a) accurate on predicting y for a given in-distribution sample x , and (b) the *confidence* $s_{\text{sup}}(x) := \max_y p(y|x)$ [23] of the classifier is *well-calibrated*, e.g., $s_{\text{sup}}(x)$ should be low when x is an OOD sample or $\arg \max_y p(y|x) \neq \text{true label}$. In our experiments, we measure the performance of s_{sup} on detecting OOD samples to evaluate a confidence-calibrated classifier.

To this end, we extend CSI with *supervised contrastive learning* (SupCLR) [31], a supervised extension of SimCLR that only contrasts different *classes* \mathcal{Y} instead of individual samples. We extend our training method (Section 2.2) to SupCLR by contrasting the *self-label augmented* [34] space $\mathcal{Y} \times \mathcal{S}$, where \mathcal{S} is the shifting transformation. In a similar manner to (3), this can be done simply by augmenting the samples via \mathcal{S} before putting into the SupCLR loss. From the learned representation, we train two types of linear classifiers: (a) $p_{\text{CSI}}(y|x)$, which predicts the class label, and (b) $p_{\text{CSI-joint}}(y, y^{\mathcal{S}}|x)$, which predicts the joint probability distribution $\mathcal{Y} \times \mathcal{S}$. We then marginalize the prediction (b) over \mathcal{S} , similarly to the ensemble score in Section 2.3, obtaining (c) $p_{\text{CSI-ens}}(y|x)$. More details on how CSI can be integrated with SupCLR are presented in Appendix B.

3 Experiments

In Section 3.1, we report OOD detection results on unlabeled one-class, unlabeled multi-class, and labeled multi-class datasets. In Section 3.2, we analyze the effects on various shifting transformations in the context of OOD detection, as well as an ablation study on each component we propose.

Table 2: AUROC (%) values of various OOD detection methods trained on unlabeled (a) CIFAR-10 and (b) ImageNet-30. * denotes the values from the reference, and bold denotes the best results.

(a) Unlabeled CIFAR-10									
Method	Network	CIFAR10 \rightarrow							
		SVHN	LSUN	ImageNet	LSUN (FIX)	ImageNet (FIX)	CIFAR-100	Interp.	
Likelihood*	PixelCNN++	8.3	-	64.2	-	-	52.6	52.6	
Likelihood*	Glow	8.3	-	66.3	-	-	58.2	58.2	
Likelihood*	EBM	63.0	-	-	-	-	-	70.0	
Likelihood Ratio* [52]	PixelCNN++	91.2	-	-	-	-	-	-	
Input Complexity* [57]	PixelCNN++	92.9	-	58.9	-	-	53.5	-	
Input Complexity* [57]	Glow	95.0	-	71.6	-	-	73.6	-	
Rot [26]	ResNet-18	97.3	87.9	89.8	76.3	82.8	78.7	63.5	
Rot+Trans [26]	ResNet-18	97.9	91.3	93.0	80.9	86.7	82.5	69.8	
GOAD [1]	ResNet-18	96.1	86.3	89.6	78.5	83.0	76.5	60.2	
CSI (ours)	ResNet-18	99.8	97.2	97.4	90.3	93.3	89.3	79.3	

(b) Unlabeled ImageNet-30									
Method	Network	ImageNet-30 \rightarrow							
		CUB-200	Dogs	Pets	Flowers	Food-101	Places-365	Caltech-256	DTD
Rot [26]	ResNet-18	77.6	76.4	69.5	87.3	75.4	50.1	70.9	90.8
Rot+Trans [26]	ResNet-18	75.0	76.0	69.0	85.9	74.0	50.1	70.3	90.6
GOAD [1]	ResNet-18	69.4	71.8	63.4	80.5	68.8	49.1	66.1	86.2
CSI (ours)	ResNet-18	90.5	96.9	84.9	94.5	89.2	78.2	86.9	96.8

Setup. We use ResNet-18 [20] architecture for all the experiments. For data augmentations, we adopt those used by Chen et al. [5]: namely, we use the combination of Inception crop [59], horizontal flip, color jitter, and grayscale as \mathcal{T} . Unless specified otherwise, we assume \mathcal{S} , the shifting transformation, to be the random rotation $0^\circ, 90^\circ, 180^\circ, 270^\circ$. We remark that one may further improve the performance by incorporating different transformations: see Table 5 for ablation study on different transformations other than rotation. By default, we train our models with the training objective in (5) and detect OOD samples with the ensembled version of the score in (9).

We mainly report the area under the receiver operating characteristic curve (AUROC) as a threshold-free evaluation metric for a detection score. In addition, we also report the test accuracy and the expected calibration error (ECE) [42, 19] for the experiments on labeled multi-class datasets. Here, ECE estimates whether a classifier can indicate when they are likely to be incorrect for test samples (from in-distribution) by measuring the difference between prediction confidence and accuracy. The formal description of the metrics and detailed experimental setups are in Appendix A.

3.1 Main results

Unlabeled one-class datasets. We start by considering the *one-class* setup: here, for a given multi-class dataset of C classes, we conduct C one-class classification tasks, where each task chooses one of the classes as in-distribution while the remaining classes being out-of-distribution. We run our experiments on three datasets, following the prior work [15, 26, 1]: CIFAR-10 [33], CIFAR-100 labeled into 20 super-classes [33], and ImageNet-30 [26] datasets. We compare our method with various prior methods including one-class classifier [56, 53], reconstruction-based [55, 48], and self-supervised [15, 26, 1] approaches. Table 1 summarizes the results, showing that CSI significantly outperforms the prior methods in all the tested cases. We provide the full, additional results, *e.g.*, class-wise results on CIFAR-100 (super-class) and ImageNet-30, in Appendix C.

Unlabeled multi-class datasets. In this setup, we assume that in-distribution samples are from a specific multi-class dataset without labels, testing on various external datasets as out-of-distribution. We compare our method on two in-distribution datasets: CIFAR-10 [33] and ImageNet-30 [26]. We consider the following datasets as out-of-distribution: SVHN [44], resized LSUN and ImageNet [38], CIFAR-100 [33], and linearly-interpolated samples of CIFAR-10 (Interp.) [12] for CIFAR-10 experiments, and CUB-200 [61], Dogs [30],

Table 3: Test accuracy (%) and AUROC (%) values of confidence-calibrated classifiers trained on labeled (a) CIFAR-10 and (b) ImageNet-30 under ResNet-18. CSI-ens denotes the ensembled prediction, *i.e.*, 4 times slower (as we use rotation) than others. Bold denotes the best results.

(a) Labeled CIFAR-10										
CIFAR10 →										
Train method	Test acc.	ECE	SVHN	LSUN	ImageNet	LSUN (FIX)	ImageNet (FIX)	CIFAR100	Interp.	
Cross Entropy	93.2	6.29	89.4	91.3	88.9	87.9	87.8	86.2	76.2	
SupCLR [31]	93.9	5.54	97.3	93.2	93.5	88.7	90.0	88.3	75.5	
CSI (ours)	94.8	4.24	96.9	96.1	96.2	91.5	92.4	90.6	78.7	
CSI-ens (ours)	96.0	3.64	98.0	97.7	97.7	93.1	94.0	92.3	80.6	

(b) Labeled ImageNet-30										
ImageNet-30 →										
Train method	Test acc.	ECE	CUB-200	Dogs	Pets	Flowers	Food-101	Places-365	Caltech-256	DTD
Cross Entropy	94.3	5.08	88.0	96.7	95.0	89.7	79.8	90.5	90.6	90.1
SupCLR [31]	96.9	3.12	86.3	95.6	94.2	92.2	81.2	89.7	90.2	92.1
CSI (ours)	97.0	2.61	93.4	97.7	96.9	96.0	87.0	92.5	91.9	93.7
CSI-ens (ours)	97.8	2.19	94.6	98.3	97.4	96.2	88.9	94.0	93.2	97.4

Pets [47], Flowers [45], Food-101 [2], Places-365 [67], Caltech-256 [18], and DTD [9] for ImageNet-30. We compare our method with various prior methods, including density-based [12, 52, 57] and self-supervised [15, 1] approaches.

Table 2 shows the results. Overall, we observe that our method significantly outperforms prior methods in all the benchmarks tested. We remark that our method is particularly effective for detecting hard (*i.e.*, near-distribution) OOD samples, *e.g.*, CIFAR-100 and Interp. in Table 2a. Also, our method still shows a notable performance in the cases when prior methods often fail, *e.g.*, Places-365 in Table 2b. Finally, we notice that the resized LSUN and ImageNet datasets officially released by Liang et al. [38] might be misleading to evaluate detection performance for hard OODs: we find that those datasets contain some unintended artifacts, due to incorrect resizing procedure. Such an artifact makes those datasets easily-detectable, *e.g.*, via input statistics. In this respect, we produce and test on their fixed versions³, coined LSUN (FIX), and ImageNet (FIX). See Appendix I for details.

Labeled multi-class datasets. We also consider the *labeled* version of the above setting: namely, we now assume that every in-distribution sample also contains discriminative label information. We use the same datasets considered in the unlabeled multi-class setup for in- and out-of-distribution datasets. We train our model as proposed in Section 2.4, and compare it with those trained by other methods, the cross-entropy and supervised contrastive learning (SupCLR) [31]. Since our goal is to calibrate the confidence, the maximum softmax probability is used to detect OOD samples (see [23]).

Table 3 shows the results. Interestingly, our method consistently improves AUROC and ECE for ImageNet-30 while maintaining test accuracy. It supports our intuition that CSI learns the discriminative information for in- vs. out-of-distribution samples, in addition to that within in-distribution. One can also observe that CSI can further improve the performance by ensembling over the transformations. We remark that our results on unlabeled datasets (in Table 2) already show comparable performance to the supervised baselines (in Table 3).

3.2 Ablation study

We perform an ablation study on various shifting transformations, training losses, and detection scores. Throughout this section, we report the mean AUROC values on one-class CIFAR-10.

Shifting transformation. We test various data transformations for the shifting transformation. In particular, we consider Cutout [11], Sobel filtering [29], Gaussian noise, Gaussian blur, and rotation [14]. We remark that

³We provide the code and datasets in <https://github.com/alinlab/CSI>.

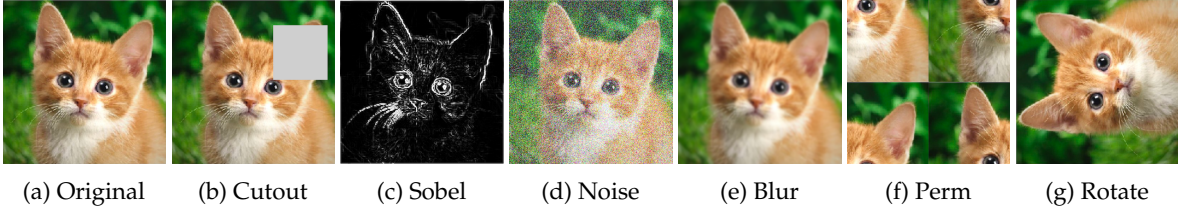


Figure 1: Visualization of the considered shifting transformations.

Table 4: AUROC (%) values of the vanilla SimCLR, using shifted in-distribution samples as OOD, trained under one-class CIFAR-10 with ResNet-18. Each column denotes the applied transformation.

	Cutout	Sobel	Noise	Blur	Perm	Rotate
AUROC	79.5	69.2	74.4	76.0	83.8	85.2

Table 5: Ablation study on various transformations, added or removed from the vanilla SimCLR. “Align” and “Shift” indicates that the transformation is used as \mathcal{T} and \mathcal{S} , respectively. (a) We add a new transformation as an aligned (up) or shifting (down) transformations. (b) We remove (up) or convert-to-shift (down) the transformation from the vanilla SimCLR. All reported values are the mean AUROC (%) over one-class CIFAR-10, and “Base” denotes the vanilla SimCLR.

(a) Add transformations							(b) Remove transformations				
Base		Cutout	Sobel	Noise	Blur	Perm	Rotate	Crop	Jitter	Gray	
87.9	+Align	84.3	85.0	85.5	88.0	73.1	76.5	-Align	55.7	78.8	78.4
	+Shift	88.5	88.3	89.3	89.2	90.7	94.3	+Shift	-	-	88.3

these transformations are reported to be ineffective in improving the class discriminative power of SimCLR [5]. In addition, we also consider the transformation coined “Perm”, which randomly permutes each part of the evenly partitioned image. Intuitively, such transformations commonly *shift* the input distribution, hence forcing them to be *aligned* can be harmful. Figure 1 visualizes all the considered transformations.

Table 4 shows AUROC values of the vanilla SimCLR, where the in-distribution samples shifted by the chosen transformation are given as OOD samples. The shifted samples are easily detected: it validates our intuition that the considered transformations *shift* the input distribution. In particular, “Perm” and “Rotate” are the most distinguishable, which implies they shift the distribution the most. Note that “Perm” and “Rotate” turns out to be the most effective shifting transformations; it implies that the transformations *shift* the distribution most indeed performs best for our method.⁴

Besides, we apply the transformation upon the vanilla SimCLR: align the transformed samples to the original samples (*i.e.*, use as \mathcal{T}) or consider them as the shifted samples (*i.e.*, use as \mathcal{S}). Table 5a shows that aligning the transformations degrade (or on par) the detection performance, while shifting the transformations gives consistent improvements. We also remove or convert-to-shift the transformation from the vanilla SimCLR in Table 5b, and see similar results. We remark that one can further improve the performance by combining multiple shifting transformations (see Appendix G).

Linear evaluation. We also measure the linear evaluation [32], the accuracy of a linear classifier to discriminate classes of in-distribution samples. It is widely used for evaluating the quality of (unsupervised) learned representation. We report the linear evaluation of vanilla SimCLR and CSI (with shifting rotation), trained under unlabeled CIFAR-10. They show comparable results, 90.48% for SimCLR and 90.19% for CSI; CSI is more specialized to learn a representation for OOD detection.

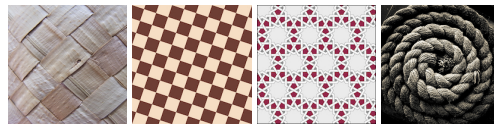
⁴We also try contrasting some *external* OOD samples in a similar manner of [25, 54]; however, we find that naïvely using them in our framework degrade the performance. This is because the contrastive loss also discriminates *within* external OOD samples, which is unnecessary and an additional learning burden for our purpose. Shifted samples can be most effective (‘nearby’ but ‘not-too-nearby’) OOD without the issue.

Table 7: Ablation study on each component of our proposed (a) training loss and (b) detection score. For (a), we use the corresponding detection score for each training loss; namely, (6) to (9) for (2) to (5), respectively. For (b), we use the model trained by the final training loss (5). We measure the mean AUROC (%) values, trained under CIFAR-10 with ResNet-18. Each row indicates the corresponding equation of the given checkmarks, and bold denotes the best results. “Con.,” “Cls.,” and “Ensem.” denotes contrast, classify, and ensemble, respectively.

(a) Training loss					(b) Detection score				
	SimCLR	Con.	Cls.	AUROC		Con.	Cls.	Ensem.	AUROC
$\mathcal{L}_{\text{SimCLR}}$ (2)	✓	-	-	87.9	s_{con} (6)	✓	-	-	91.3
$\mathcal{L}_{\text{con-SI}}$ (3)	✓	✓	-	91.6	$s_{\text{con-SI}}$ (7)	✓	-	✓	93.3
$\mathcal{L}_{\text{cls-SI}}$ (4)	-	-	✓	88.6	$s_{\text{cls-SI}}$ (8)	-	✓	✓	93.8
\mathcal{L}_{CSI} (5)	✓	✓	✓	94.3	s_{CSI} (9)	✓	✓	✓	94.3

Data-dependence of shifting transformation. We remark that the best choice of shifting transformation for detecting OODs depends on the dataset. For instance, consider a rotation-invariant dataset such as texture. Here, the rotation should not be a shifting transformation. Table 6 shows the AUROC values where Describable Textures Dataset (DTD) [9] and ImageNet-30 are in- and out-of-distribution samples, respectively. We compare the vanilla SimCLR and CSI using rotation as \mathcal{S} , denoted as “Base”, and “CSI (Rotation)”, respectively. Unlike natural images, shifting rotated images degrades OOD detection. See Appendix J for additional discussion.

Table 6: AUROC (%) on DTD dataset, where ImageNet-30 is used for OOD.



Base	CSI (Rotation)
92.9	65.4

Training loss. In Table 7a, we assess the individual effects of each component that consists of our final training loss (5): namely, we compare the vanilla SimCLR (2), contrasting shifted instances (3), and classifying shifted instances (4) losses. For the evaluation of the models of different training losses (2) to (5), we use the detection scores defined in (6) to (9), respectively. We remark that both contrasting and classifying shows better results than the vanilla SimCLR; and combining them (*i.e.*, the final CSI loss (5)) gives further improvements, *i.e.*, two losses are complementary.

Detection score. Finally, Table 7b shows the effect of each component in our detection score: the vanilla contrastive (6), contrasting shifted instances (7), and classifying shifted instances (8) scores. We ensemble the scores over both \mathcal{T} and \mathcal{S} for (7) to (9), and use a single sample for (6). All the reported values are evaluated from the model trained by the final loss 5. Similar to above, both contrasting and classifying scores show better results than the vanilla contrastive score; and combining them (*i.e.*, the final CSI score (9)) gives further improvements.

4 Related work

4.1 OOD detection

Out-of-distribution (OOD) detection is a classic and essential problem in machine learning, studied under different names, *e.g.*, novelty or anomaly detection [27]. In this paper, we primarily focus on *unsupervised* OOD detection, which is arguably the most traditional and popular setup in the field [56]. In this setting, the detector is only allowed to access in-distribution samples while required to identify unseen OOD samples. There are other settings, *e.g.*, semi-supervised setting - the detector can access a small subset of out-of-distribution samples [25, 54], or supervised setting - the detector knows the target out-of-distribution, but we do not consider those settings in this paper. We remark that the unsupervised setting is the most practical and challenging scenario since there are *infinitely* many cases for out-of-distribution, and it is often not possible to have such external data.

Most recent works can be grouped into four categories: (a) density-based [66, 43, 7, 12, 52, 57, 17], (b) reconstruction-based [55, 68, 10, 50, 48, 8], (c) one-class classifier [56, 53], and (d) self-supervised [15, 26, 1] methods. We note that there are more extensive literature on this topic, but we mainly focus on the recent work based on deep learning due to the limited space (see [27, 4, 51] for survey). Brief description for each method are as follows:

- **Density-based methods.** Density-based methods are one of the most classic and principled approaches for OOD detection. Intuitively, they directly use the likelihood of the sample as the detection score. However, recent studies reveal that the likelihood is often not the best metric - especially for deep neural networks with complex datasets [43, 7]. Several work thus proposed modified scores, *e.g.*, WAIC [7], likelihood ratio [52], and input complexity [57], or utilized unnormalized likelihood (*i.e.*, energy) [12, 17].
- **Reconstruction-based methods.** Reconstruction-based approach is another popular line of research for OOD detection. It trains an encoder-decoder network that reconstructs the training data in an unsupervised manner. Since the encoder-decoder network would less generalize for unseen OOD samples, they use the reconstruction loss as the detection score. There are also several works on this approach, utilizing generative auto-encoders [68, 50] or generative adversarial networks [55, 10, 48].
- **One-class classifiers.** One-class classifiers are also a classic and principled approach for OOD detection. They learn a decision boundary of in- vs. out-of-distribution samples, by giving some margin that covers the in-distribution samples [56]. Recent work shows that the one-class classifier is effective upon the deep representation [53].
- **Self-supervised methods.** Self-supervised methods are a relatively new approach based on the strong representation learned from the self-supervision [14]. They train a network with a pre-defined task (*e.g.*, predict the angle of the rotated image) on the training set, and use the generalization error to detect OOD samples. Recent self-supervised methods show outstanding results on various OOD detection benchmark datasets [15, 26, 1].

Our work can be categorized into the self-supervised methods, but differs from the prior work as we consider the *contrastive learning* type of self-supervision [5]. We validate the power of contrastive representation learning can be extended for OOD detection, with proper modification.

4.2 Confidence-calibrated classifiers

Another line of research is on confidence-calibrated classifiers [23], which relaxes the overconfidence issues of the classifiers. There are two types of calibration: (a) *in-distribution* calibration, that aligns the uncertainty and the actual accuracy, measured by ECE [42, 19], and (b) *out-of-distribution* detection, that reduces the uncertainty of OOD samples, measured by AUROC [23, 36]. Note that the goal of confidence-calibrated classifiers is to regularize the prediction; hence all three tasks: classification, in-distribution calibration, and out-of-distribution detection, are done by the softmax probability. Namely, the detection score is given by the confidence (or maximum softmax probability) [23]. There are also several works on designing a specific detection score utilizing the pre-trained classifier (*e.g.*, [38, 37]), but we do not consider those approaches in this paper.

4.3 Self-supervised learning

Self-supervised learning [14, 32] show remarkable success in learning representation recently. In particular, contrastive learning [46], specifically instance discrimination [62], show the state-of-the-art results on visual representation learning [21, 5]. However, most prior works primarily focus on improving the downstream task performance (*e.g.*, classification); and other advantages of self-supervised learning (*e.g.*, uncertainty or robustness) are rarely investigated [26]. Our work first verifies the effectiveness of contrastive learning for OOD detection.

5 Conclusion

We propose a simple yet effective method named contrasting shifted instances (CSI), which extends the power of contrastive learning for out-of-distribution (OOD) detection problems. CSI demonstrates outstanding performance under various OOD detection scenarios. We believe our work would guide various future directions in OOD detection and self-supervised learning as an important baseline.

References

- [1] L. Bergman and Y. Hoshen. Classification-based anomaly detection for general data. In *International Conference on Learning Representations*, 2020.
- [2] L. Bossard, M. Guillaumin, and L. Van Gool. Food-101—mining discriminative components with random forests. In *European Conference on Computer Vision*, 2014.
- [3] R. Caruana, Y. Lou, J. Gehrke, P. Koch, M. Sturm, and N. Elhadad. Intelligible models for healthcare: Predicting pneumonia risk and hospital 30-day readmission. In *ACM SIGKDD International Conference on Knowledge Discovery and Data Mining*, 2015.
- [4] V. Chandola, A. Banerjee, and V. Kumar. Anomaly detection: A survey. *ACM computing surveys (CSUR)*, 2009.
- [5] T. Chen, S. Kornblith, M. Norouzi, and G. Hinton. A simple framework for contrastive learning of visual representations. *arXiv preprint arXiv:2002.05709*, 2020.
- [6] X. Chen, H. Fan, R. Girshick, and K. He. Improved baselines with momentum contrastive learning. *arXiv preprint arXiv:2003.04297*, 2020.
- [7] H. Choi, E. Jang, and A. A. Alemi. Waic, but why? generative ensembles for robust anomaly detection. *arXiv preprint arXiv:1810.01392*, 2018.
- [8] S. Choi and S.-Y. Chung. Novelty detection via blurring. In *International Conference on Learning Representations*, 2020.
- [9] M. Cimpoi, S. Maji, I. Kokkinos, S. Mohamed, and A. Vedaldi. Describing textures in the wild. In *IEEE Conference on Computer Vision and Pattern Recognition*, 2014.
- [10] L. Deecke, R. Vandermeulen, L. Ruff, S. Mandt, and M. Kloft. Image anomaly detection with generative adversarial networks. In *Joint European Conference on Machine Learning and Knowledge Discovery in Databases*, 2018.
- [11] T. DeVries and G. W. Taylor. Improved regularization of convolutional neural networks with cutout. *arXiv preprint arXiv:1708.04552*, 2017.
- [12] Y. Du and I. Mordatch. Implicit generation and modeling with energy based models. In *Advances in Neural Information Processing Systems*, 2019.
- [13] K. Eykholt, I. Evtimov, E. Fernandes, B. Li, A. Rahmati, C. Xiao, A. Prakash, T. Kohno, and D. Song. Robust physical-world attacks on deep learning visual classification. In *IEEE Conference on Computer Vision and Pattern Recognition*, 2018.
- [14] S. Gidaris, P. Singh, and N. Komodakis. Unsupervised representation learning by predicting image rotations. In *International Conference on Learning Representations*, 2018.
- [15] I. Golan and R. El-Yaniv. Deep anomaly detection using geometric transformations. In *Advances in Neural Information Processing Systems*, 2018.

- [16] P. Goyal, P. Dollár, R. Girshick, P. Noordhuis, L. Wesolowski, A. Kyrola, A. Tulloch, Y. Jia, and K. He. Accurate, large minibatch sgd: Training imagenet in 1 hour. *arXiv preprint arXiv:1706.02677*, 2017.
- [17] W. Grathwohl, K.-C. Wang, J.-H. Jacobsen, D. Duvenaud, M. Norouzi, and K. Swersky. Your classifier is secretly an energy based model and you should treat it like one. In *International Conference on Learning Representations*, 2020.
- [18] G. Griffin, A. Holub, and P. Perona. Caltech-256 object category dataset, 2007.
- [19] C. Guo, G. Pleiss, Y. Sun, and K. Q. Weinberger. On calibration of modern neural networks. In *International Conference on Machine Learning*, 2017.
- [20] K. He, X. Zhang, S. Ren, and J. Sun. Deep residual learning for image recognition. In *IEEE Conference on Computer Vision and Pattern Recognition*, 2016.
- [21] K. He, H. Fan, Y. Wu, S. Xie, and R. Girshick. Momentum contrast for unsupervised visual representation learning. *arXiv preprint arXiv:1911.05722*, 2019.
- [22] O. J. Hénaff, A. Srinivas, J. De Fauw, A. Razavi, C. Doersch, S. Eslami, and A. v. d. Oord. Data-efficient image recognition with contrastive predictive coding. *arXiv preprint arXiv:1905.09272*, 2019.
- [23] D. Hendrycks and K. Gimpel. A baseline for detecting misclassified and out-of-distribution examples in neural networks. In *International Conference on Learning Representations*, 2017.
- [24] D. Hendrycks, K. Lee, and M. Mazeika. Using pre-training can improve model robustness and uncertainty. In *International Conference on Machine Learning*, 2019.
- [25] D. Hendrycks, M. Mazeika, and T. Dietterich. Deep anomaly detection with outlier exposure. In *International Conference on Learning Representations*, 2019.
- [26] D. Hendrycks, M. Mazeika, S. Kadavath, and D. Song. Using self-supervised learning can improve model robustness and uncertainty. In *Advances in Neural Information Processing Systems*, 2019.
- [27] V. Hodge and J. Austin. A survey of outlier detection methodologies. *Artificial intelligence review*, 2004.
- [28] S. Ioffe and C. Szegedy. Batch normalization: Accelerating deep network training by reducing internal covariate shift. *International Conference on Machine Learning*, 2015.
- [29] N. Kanopoulos, N. Vasanthavada, and R. L. Baker. Design of an image edge detection filter using the sobel operator. *IEEE Journal of solid-state circuits*, 1988.
- [30] A. Khosla, N. Jayadevaprakash, B. Yao, and L. Fei-Fei. Novel dataset for fine-grained image categorization. In *IEEE Conference on Computer Vision and Pattern Recognition*, Colorado Springs, CO, June 2011.
- [31] P. Khosla, P. Teterwak, C. Wang, A. Sarna, Y. Tian, P. Isola, A. Maschinot, C. Liu, and D. Krishnan. Supervised contrastive learning. *arXiv preprint arXiv:2004.11362*, 2020.
- [32] A. Kolesnikov, X. Zhai, and L. Beyer. Revisiting self-supervised visual representation learning. In *IEEE Conference on Computer Vision and Pattern Recognition*, 2019.
- [33] A. Krizhevsky et al. Learning multiple layers of features from tiny images, 2009.
- [34] H. Lee, S. J. Hwang, and J. Shin. Rethinking data augmentation: Self-supervision and self-distillation. *arXiv preprint arXiv:1910.05872*, 2019.
- [35] K. Lee, C. Hwang, K. S. Park, and J. Shin. Confident multiple choice learning. In *International Conference on Machine Learning*, 2017.
- [36] K. Lee, H. Lee, K. Lee, and J. Shin. Training confidence-calibrated classifiers for detecting out-of-distribution samples. In *International Conference on Learning Representations*, 2018.

- [37] K. Lee, K. Lee, H. Lee, and J. Shin. A simple unified framework for detecting out-of-distribution samples and adversarial attacks. In *Advances in Neural Information Processing Systems*, 2018.
- [38] S. Liang, Y. Li, and R. Srikant. Enhancing the reliability of out-of-distribution image detection in neural networks. In *International Conference on Learning Representations*, 2018.
- [39] I. Loshchilov and F. Hutter. Sgdr: Stochastic gradient descent with warm restarts. *arXiv preprint arXiv:1608.03983*, 2016.
- [40] L. v. d. Maaten and G. Hinton. Visualizing data using t-sne. *Journal of machine learning research*, 2008.
- [41] J. MacQueen et al. Some methods for classification and analysis of multivariate observations, 1967.
- [42] M. P. Naeni, G. Cooper, and M. Hauskrecht. Obtaining well calibrated probabilities using bayesian binning. In *AAAI Conference on Artificial Intelligence*, 2015.
- [43] E. Nalisnick, A. Matsukawa, Y. W. Teh, D. Gorur, and B. Lakshminarayanan. Do deep generative models know what they don't know? In *International Conference on Learning Representations*, 2019.
- [44] Y. Netzer, T. Wang, A. Coates, A. Bissacco, B. Wu, and A. Y. Ng. Reading digits in natural images with unsupervised feature learning. In *Advances in Neural Information Processing Systems Workshop on Deep Learning and Unsupervised Feature Learning*, 2011.
- [45] M.-E. Nilsback and A. Zisserman. A visual vocabulary for flower classification. In *IEEE Conference on Computer Vision and Pattern Recognition*, 2006.
- [46] A. v. d. Oord, Y. Li, and O. Vinyals. Representation learning with contrastive predictive coding. *arXiv preprint arXiv:1807.03748*, 2018.
- [47] O. M. Parkhi, A. Vedaldi, A. Zisserman, and C. Jawahar. Cats and dogs. In *IEEE Conference on Computer Vision and Pattern Recognition*, 2012.
- [48] P. Perera, R. Nallapati, and B. Xiang. Ocgan: One-class novelty detection using gans with constrained latent representations. In *IEEE Conference on Computer Vision and Pattern Recognition*, 2019.
- [49] C. Phua, V. Lee, K. Smith, and R. Gayler. A comprehensive survey of data mining-based fraud detection research. *arXiv preprint arXiv:1009.6119*, 2010.
- [50] S. Pidhorskyi, R. Almoheisen, and G. Doretto. Generative probabilistic novelty detection with adversarial autoencoders. In *Advances in Neural Information Processing Systems*, 2018.
- [51] M. A. Pimentel, D. A. Clifton, L. Clifton, and L. Tarassenko. A review of novelty detection. *Signal Processing*, 2014.
- [52] J. Ren, P. J. Liu, E. Fertig, J. Snoek, R. Poplin, M. Depristo, J. Dillon, and B. Lakshminarayanan. Likelihood ratios for out-of-distribution detection. In *Advances in Neural Information Processing Systems*, 2019.
- [53] L. Ruff, R. Vandermeulen, N. Goernitz, L. Deecke, S. A. Siddiqui, A. Binder, E. Müller, and M. Kloft. Deep one-class classification. In *International Conference on Machine Learning*, 2018.
- [54] L. Ruff, R. A. Vandermeulen, N. Görnitz, A. Binder, E. Müller, K.-R. Müller, and M. Kloft. Deep semi-supervised anomaly detection. In *International Conference on Learning Representations*, 2020.
- [55] T. Schlegl, P. Seeböck, S. M. Waldstein, U. Schmidt-Erfurth, and G. Langs. Unsupervised anomaly detection with generative adversarial networks to guide marker discovery. In *International conference on information processing in medical imaging*, 2017.
- [56] B. Schölkopf, R. C. Williamson, A. J. Smola, J. Shawe-Taylor, and J. C. Platt. Support vector method for novelty detection. In *Advances in Neural Information Processing Systems*, 2000.

- [57] J. Serrà, D. Álvarez, V. Gómez, O. Slizovskaia, J. F. Núñez, and J. Luque. Input complexity and out-of-distribution detection with likelihood-based generative models. In *International Conference on Learning Representations*, 2020.
- [58] A. Srinivas, M. Laskin, and P. Abbeel. Curl: Contrastive unsupervised representations for reinforcement learning. *arXiv preprint arXiv:2004.04136*, 2020.
- [59] C. Szegedy, W. Liu, Y. Jia, P. Sermanet, S. Reed, D. Anguelov, D. Erhan, V. Vanhoucke, and A. Rabinovich. Going deeper with convolutions. In *IEEE Conference on Computer Vision and Pattern Recognition*, pages 1–9, 2015.
- [60] Y. Tian, D. Krishnan, and P. Isola. Contrastive multiview coding. *arXiv preprint arXiv:1906.05849*, 2019.
- [61] C. Wah, S. Branson, P. Welinder, P. Perona, and S. Belongie. The Caltech-UCSD Birds-200-2011 Dataset. Technical Report CNS-TR-2011-001, California Institute of Technology, 2011.
- [62] Z. Wu, Y. Xiong, S. X. Yu, and D. Lin. Unsupervised feature learning via non-parametric instance discrimination. In *IEEE Conference on Computer Vision and Pattern Recognition*, 2018.
- [63] G.-S. Xia, X. Bai, J. Ding, Z. Zhu, S. Belongie, J. Luo, M. Datcu, M. Pelillo, and L. Zhang. Dots: A large-scale dataset for object detection in aerial images. In *IEEE Conference on Computer Vision and Pattern Recognition*, 2018.
- [64] Y. You, I. Gitman, and B. Ginsburg. Large batch training of convolutional networks. *arXiv preprint arXiv:1708.03888*, 2017.
- [65] S. Yun, J. Park, K. Lee, and J. Shin. Regularizing class-wise predictions via self-knowledge distillation. In *IEEE Conference on Computer Vision and Pattern Recognition*, 2020.
- [66] S. Zhai, Y. Cheng, W. Lu, and Z. Zhang. Deep structured energy based models for anomaly detection. In *International Conference on Machine Learning*, 2016.
- [67] B. Zhou, A. Lapedriza, A. Khosla, A. Oliva, and A. Torralba. Places: A 10 million image database for scene recognition. *IEEE Transactions on Pattern Analysis and Machine Intelligence*, 2017.
- [68] B. Zong, Q. Song, M. R. Min, W. Cheng, C. Lumezanu, D. Cho, and H. Chen. Deep autoencoding gaussian mixture model for unsupervised anomaly detection. In *International Conference on Learning Representations*, 2018.

Appendix

CSI: Novelty Detection via Contrastive Learning on Distributionally Shifted Instances

A Experimental details

Training details. We use ResNet-18 [20] as the base encoder network f_θ and 2-layer multi-layer perceptron with 128 embedding dimension as the projection head g_ϕ . All models are trained by minimizing the final loss \mathcal{L}_{CSI} (5) with a temperature of $\tau = 0.5$. We follow the same optimization step of SimCLR [5]. For optimization, we train CSI with 1,000 epoch under LARS optimizer [64] with weight decay of $1e-6$ and momentum with 0.9. For the learning rate scheduling, we use linear warmup [16] for early 10 epochs until learning rate of 1.0 and decay with cosine decay schedule without a restart [39]. We use batch size of 512 for both vanilla SimCLR and ours: where the batch is given by \mathcal{B} for vanilla SimCLR and the aggregated one $\cup_{S \in \mathcal{S}} \mathcal{B}_S$ for ours. Furthermore, we use global batch normalization (BN) [28], which shares the BN parameters (mean and variance) over the GPUs in distributed training.

For supervised contrastive learning (SupCLR) [31] and supervised CSI, we select the best temperature from $\{0.07, 0.5\}$: SupCLR recommend 0.07 but 0.5 was better in our experiments. For training the encoder f_θ , we use the same optimization scheme as above, except using 700 for the epoch. For training the linear classifier, we train the model for 100 epochs with batch size 128, using stochastic gradient descent with momentum 0.9. The learning rate starts at 0.1 and is dropped by a factor of 10 at 60%, 75%, and 90% of the training progress.

Data augmentation details. We use SimCLR augmentations: Inception crop [59], horizontal flip, color jitter, and grayscale for random augmentations \mathcal{T} , and rotation as shifting transformation \mathcal{S} . The detailed description of the augmentations are as follows:

- **Inception crop.** Randomly crops the area of the original image with uniform distribution 0.08 to 1.0. After the crop, cropped image are resized to the original image size.
- **Horizontal flip.** Flips the image horizontally with 50% of probability.
- **Color jitter.** Change the hue, brightness, and saturation of the image. We transform the RGB (red, green, blue) image into an HSV (hue, saturation, value) image format and add noise to the HSV channels. We apply color jitter with 80% of probability.
- **Grayscale.** Convert into a gray image. Randomly apply a grayscale with 20% of probability.
- **Rotation.** We use rotation as \mathcal{S} , the shifting transformation, $\{0^\circ, 90^\circ, 180^\circ, 270^\circ\}$. For a given batch \mathcal{B} , we apply each rotation degree to obtain the new batch for CSI: $\cup_{S \in \mathcal{S}} \mathcal{B}_S$.

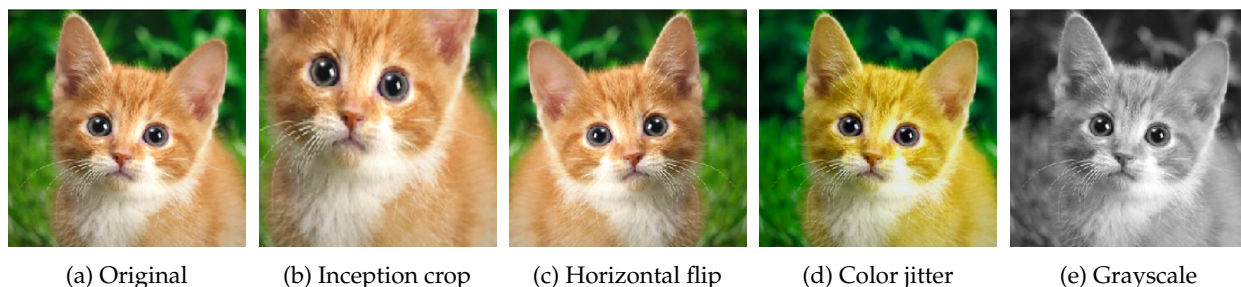


Figure 2: Visualization of original image and SimCLR augmentations.

Dataset details. For one-class datasets, we train one class of CIFAR-10 [33], CIFAR-100 (super-class) [33], and ImageNet-30 [26]. CIFAR-10 and CIFAR-100 consist of 50,000 training and 10,000 test images with 10 and 20 (super-class) image classes, respectively. ImageNet-30 contains 39,000 training and 3,000 test images with 30 image classes.

For unlabeled and labeled multi-class datasets, we train ResNet with CIFAR-10 and ImageNet-30. For CIFAR-10, out-of-distribution (OOD) samples are as follows: SVHN [44] consists of 26,032 test images with 10 digits, resized LSUN [38] consists of 10,000 test images of 10 different scenes, resized ImageNet [38] consists of 10,000 test images with 200 images classes from a subset of full ImageNet dataset, Interp. consists of 10,000 test images of linear interpolation of CIFAR-10 test images, and LSUN (FIX), ImageNet (FIX) consists of 10,000 test images, respectively with following details in Appendix I. For multi-class ImageNet-30, OOD samples are as follows: CUB-200 [61], Stanford Dogs [30], Oxford Pets [47], Oxford Flowers [45], Food-101 [2] without the “hotdog” class to avoid overlap, Places-365 [67] with small images (256 * 256) validation set, Caltech-256 [18], and Describable Textures Dataset (DTD) [9]. Here, we randomly sample 3,000 images to balance with the in-distribution test set.

Evaluation metrics. For evaluation, we measure the two metrics that each measures (a) the effectiveness of the proposed score in distinguishing in- and out-of-distribution images, (b) the confidence calibration of softmax classifier.

- **Area under the receiver operating characteristic curve (AUROC).** Let TP, TN, FP, and FN denote true positive, true negative, false positive and false negative, respectively. The ROC curve is a graph plotting true positive rate = TP / (TP+FN) against the false positive rate = FP / (FP+TN) by varying a threshold.
- **Expected calibration error (ECE).** For a given test data $\{(x_n, y_n)\}_{n=1}^N$, we group the predictions into M interval bins (each of size $1/M$). Let B_m be the set of indices of samples whose prediction confidence falls into the interval $(\frac{m-1}{M}, \frac{m}{M}]$. Then, the expected calibration error (ECE) [42, 19] is follows:

$$\text{ECE} = \sum_{m=1}^M \frac{|B_m|}{N} |\text{acc}(B_m) - \text{conf}(B_m)|, \quad (10)$$

where $\text{acc}(B_m)$ is accuracy of B_m : $\text{acc}(B_m) = \frac{1}{|B_m|} \sum_{i \in B_m} \mathbb{1}_{\{y_i = \arg \max_y p(y|x_i)\}}$ where $\mathbb{1}$ is indicator function and $\text{conf}(B_m)$ is confidence of B_m : $\text{conf}(B_m) = \frac{1}{|B_m|} \sum_{i \in B_m} q(x_i)$ where $q(x_i)$ is the confidence of data x_i .

B Detailed description for confidence-calibrated classifiers

We propose a simple extension of CSI for training a *confidence-calibrated* classifier [23]. To this end, we first explain the supervised contrastive learning (SupCLR) [31], a supervised extension of SimCLR that contrasts the samples of *different classes* instead of the different samples. Following the notation of SimCLR, let $\mathcal{C} = \{(x_i, y_i)\}_{i=1}^B$ be a training batch with class labels $y_i \in \mathcal{Y}$, and $\tilde{\mathcal{C}}$ be an augmented batch with class labels, *i.e.*, $\tilde{\mathcal{C}} := \{(\tilde{x}_i, y_i) \mid \tilde{x}_i \in \tilde{\mathcal{B}}\}$. We define a subset of $\tilde{\mathcal{C}}$ with the samples of label y , namely, $\tilde{\mathcal{C}}_y := \{(\tilde{x}_i, y_i) \in \tilde{\mathcal{C}} \mid y = y_i\}$. Then, the SupCLR objective is:

$$\mathcal{L}_{\text{SupCLR}}(\mathcal{C}) := \frac{1}{2B} \sum_{i=1}^B \mathcal{L}_{\text{con}}(\tilde{x}_i^{(1)}, \tilde{\mathcal{C}}_{y_i} \setminus \{\tilde{x}_i^{(1)}\}, \tilde{\mathcal{C}}_{-y_i}) + \mathcal{L}_{\text{con}}(\tilde{x}_i^{(2)}, \tilde{\mathcal{C}}_{y_i} \setminus \{\tilde{x}_i^{(2)}\}, \tilde{\mathcal{C}}_{-y_i}) \quad (11)$$

where \setminus denotes the set complement and $\tilde{\mathcal{C}}_{-y_i} := \tilde{\mathcal{C}} \setminus \tilde{\mathcal{C}}_{y_i}$. After learning representation with the SupCLR objective (11), we train a linear classifier $p_{\text{SupCLR}}(y|x)$ which predicts the class labels, upon the embedding network $f_{\theta}(x)$. Here, we use the *confidence* (or maximum softmax probability) [23] $s_{\text{sup}}(x) := \max_y p(y|x)$ where p is given by p_{SupCLR} to detect OOD samples.

Similar to the contrasting loss for SimCLR (3), we extend the SupCLR objective utilizing the shifting transformations \mathcal{S} . To this end, we consider the joint label $(y, y^{\mathcal{S}}) \in \mathcal{Y} \times \mathcal{S}$ of class label y and shifting

transformation y^S . Let $\mathcal{C}_S := \{(S(x_i), (y_i, S))\}$ be the shifted batch for each transformation $S \in \mathcal{S}$. Then, the supervised contrasting shifted instances (sup-CSI) loss is given by

$$\mathcal{L}_{\text{sup-CSI}} := \mathcal{L}_{\text{SupCLR}} \left(\bigcup_{S \in \mathcal{S}} \mathcal{C}_S \right), \quad (12)$$

defined on the *self-label augmented* [34] space $\mathcal{Y} \times \mathcal{S}$. We observe that the classifying shifted instances loss $\mathcal{L}_{\text{cls-SI}}$ (7) do not help supervised learning, which coincides with the observation of [34] that the self-supervised labels often conflict with the class labels. Hence, we only use the contrasting shifted instances loss $\mathcal{L}_{\text{con-SI}}$ (3) for our supervised experiments.

From the learned representation, we train two types of linear classifiers: (a) $p_{\text{CSI}}(y|x)$, which predicts the class labels, and (b) $p_{\text{CSI-joint}}(y, y^S|x)$, which predicts the joint labels. For the former one, we use $p_{\text{CSI}}(y|x)$ directly to compute the confidence $s_{\text{sup}}(x)$. For the latter one, we marginalize the joint prediction over the shifting transformation similar to Section 2.3. Formally, let $l(x) \in \mathbb{R}^{C \times K}$ be the logit values of $p_{\text{CSI-joint}}(y, y^S|x)$ where $|\mathcal{Y}| = C$ and $|\mathcal{S}| = K$. Let $l(x)_k \in \mathbb{R}^C$ denote the logit values correspond to $p_{\text{CSI-joint}}(y, y^S = S_k|x)$. Then, the ensembled probability is given by:

$$p_{\text{CSI-ens}}(y|x) := \sigma \left(\frac{1}{K} \sum_k l(S_k(x))_k \right), \quad (13)$$

where σ denotes the softmax activation. Here, we use $p_{\text{CSI-ens}}$ to compute the confidence $s_{\text{sup}}(x)$. We denote the confidence computed by p_{CSI} and $p_{\text{CSI-ens}}$ and ‘‘CSI’’ and ‘‘CSI-ens’’, respectively.

C Additional one-class OOD detection results

Table 8 presents the confusion matrix of AUROC values of our method on one-class CIFAR-10 datasets, where bold denotes the hard pairs. The results align with the human intuition that ‘car’ is confused to ‘ship’ and ‘truck’, and ‘cat’ is confused to ‘dog’.

Table 9 presents the OOD detection results of various methods on one-class CIFAR-100 (super-class) datasets, for all 20 super-classes. Our method outperforms the prior methods for all classes.

Table 10 presents the OOD detection results of our method on one-class ImageNet-30 dataset, for all 30 classes. Our method consistently performs well for all classes.

Table 8: Confusion matrix of AUROC (%) values of our method on one-class CIFAR-10. The row and column indicates the in-distribution and OOD class, respectively, and the final column indicates the mean value. Bold denotes the values under 80%, which implies the hard pair.

	Plane	Car	Bird	Cat	Deer	Dog	Frog	Horse	Ship	Truck	Mean
Plane	-	74.1	95.8	98.4	94.9	98.0	96.2	90.1	79.6	82.8	90.0
Car	99.3	-	99.9	99.9	99.8	99.9	99.8	99.7	98.7	95.0	99.1
Bird	91.1	97.5	-	97.3	87.0	92.5	96.1	83.2	96.4	98.0	93.2
Cat	91.9	91.5	90.3	-	83.3	67.0	89.6	79.0	92.8	91.9	86.4
Deer	95.7	98.4	94.9	96.6	-	94.7	98.7	69.0	97.4	98.8	93.8
Dog	97.9	98.5	95.5	90.3	88.1	-	96.8	76.6	98.6	98.3	93.4
Frog	93.6	92.3	94.6	96.1	96.8	96.3	-	95.2	94.4	97.3	95.2
Horse	99.3	99.5	99.0	99.3	94.2	97.4	99.8	-	99.7	99.4	98.6
Ship	96.6	91.2	99.5	99.7	99.4	99.7	99.5	99.3	-	96.6	97.9
Truck	96.2	72.3	99.4	99.5	99.1	99.4	98.7	98.3	96.2	-	95.5

Table 9: AUROC (%) values of various OOD detection methods trained on one-class CIFAR-100 (super-class). Each row indicates the results of the selected super-class, and the final row indicates the mean value. * denotes the values from the reference, and bold denotes the best results.

	OC-SVM*	DAGMM*	DSEBM*	ADGAN*	Geom*	Rot	Rot+Trans	GOAD	CSI (ours)
0	68.4	43.4	64.0	63.1	74.7	78.6	79.6	73.9	86.3
1	63.6	49.5	47.9	64.9	68.5	73.4	73.3	69.2	84.8
2	52.0	66.1	53.7	41.3	74.0	70.1	71.3	67.6	88.9
3	64.7	52.6	48.4	50.0	81.0	68.6	73.9	71.8	85.7
4	58.2	56.9	59.7	40.6	78.4	78.7	79.7	72.7	93.7
5	54.9	52.4	46.6	42.8	59.1	69.7	72.6	67.0	81.9
6	57.2	55.0	51.7	51.1	81.8	78.8	85.1	80.0	91.8
7	62.9	52.8	54.8	55.4	65.0	62.5	66.8	59.1	83.9
8	65.6	53.2	66.7	59.2	85.5	84.2	86.0	79.5	91.6
9	74.1	42.5	71.2	62.7	90.6	86.3	87.3	83.7	95.0
10	84.1	52.7	78.3	79.8	87.6	87.1	88.6	84.0	94.0
11	58.0	46.4	62.7	53.7	83.9	76.2	77.1	68.7	90.1
12	68.5	42.7	66.8	58.9	83.2	83.3	84.6	75.1	90.3
13	64.6	45.4	52.6	57.4	58.0	60.7	62.1	56.6	81.5
14	51.2	57.2	44.0	39.4	92.1	87.1	88.0	83.8	94.4
15	62.8	48.8	56.8	55.6	68.3	69.0	71.9	66.9	85.6
16	66.6	54.4	63.1	63.3	73.5	71.7	75.6	67.5	83.0
17	73.7	36.4	73.0	66.7	93.8	92.2	93.5	91.6	97.5
18	52.8	52.4	57.7	44.3	90.7	90.4	91.5	88.0	95.9
19	58.4	50.3	55.5	53.0	85.0	86.5	88.1	82.6	95.2
Mean	63.1	50.6	58.8	55.2	78.7	77.7	79.8	74.5	89.6

Table 10: AUROC (%) values of our method trained on one-class ImageNet-30. The first and third row indicates the selected class, and the second and fourth row indicates the corresponding results.

0	1	2	3	4	5	6	7	8	9	10	11	12	13	14
85.9	99.0	99.8	90.5	95.8	99.2	96.6	83.5	92.2	84.3	99.0	94.5	97.1	87.7	96.4
15	16	17	18	19	20	21	22	23	24	25	26	27	28	29
84.7	99.7	75.6	95.2	73.8	94.7	95.2	99.2	98.5	82.5	89.7	82.1	97.2	82.1	97.6

D Ablation study on random augmentation

We verify that ensembling the scores over the random augmentations \mathcal{T} improves OOD detection. However, naïve random sampling from the entire \mathcal{T} is often sample inefficient. We find that choosing a proper subset $\mathcal{T}_{\text{control}} \subset \mathcal{T}$ improves the performance for given number of samples. Specifically, we choose $\mathcal{T}_{\text{control}}$ as the set of the *most common* samples. For example, the size of the cropping area is sampled from $\mathcal{U}[0.08, 1]$ for uniform distribution \mathcal{U} during training. Since the rare samples, *e.g.*, area near 0.08 increases the noise, we only use the samples with size $(0.08 + 1)/2 = 0.54$ during inference. Table 11 shows random sampling from the controlled set often gives improvements.

Table 11: AUROC (%) values of our method for different number of random augmentations, under one-class (OC-) CIFAR-10 and CIFAR-100 (super-class). The values are averaged over classes. Random augmentations over the controlled set show the best performance.

# of samples	Controlled	OC-CIFAR-10	OC-CIFAR-100
4	-	92.22	87.36
40	-	94.13	89.51
40	✓	94.31	89.55

E Efficient computation of (6) via coresets

One can reduce the computation and memory cost of the contrastive score (6) by selecting a proper subset, *i.e.*, *coreset*, of the training samples. To this end, we run K-means clustering [41] on the normalized features $W_m := z(x_m)/\|z(x_m)\|$ using cosine similarity as a metric. Then, we use the center of each cluster as the coreset. For contrasting shifted instances (4), we choose the coreset for each shifting transformation S . Table 12 shows the results for various coreset sizes, given by a ratio from the full training samples. Keeping only a few (*e.g.*, 1%) samples is sufficient.

Table 12: AUROC (%) values of our method for various coreset sizes (% of training samples), under one-class (OC-) CIFAR-10, CIFAR-100 (super-class), and ImageNet-30. The values are averaged over classes. Keeping only a few (*e.g.*, 1%) samples shows sufficiently good results.

Coreset (%)	OC-CIFAR-10	OC-CIFAR-100	OC-ImageNet-30
1%	94.22	89.27	91.06
10%	94.30	89.46	91.51
100%	94.31	89.55	91.63

F Ablation study on the balancing terms

We study the effects of the balancing terms λ_S^{con} , λ_S^{cls} in Section 2.3. To this end, we compare of our final loss (5), without (w/o) and with (w/) the balancing terms λ_S^{con} and λ_S^{cls} . When not using the balancing terms, we set $\lambda_S^{\text{con}} = \lambda_S^{\text{cls}} = 1$ for all S . We follow the experimental setup of Table 1, *e.g.*, use rotation for the shifting transformation. We run our experiments on CIFAR-10, CIFAR-100 (super-class), and ImageNet-30 datasets. Table 13 shows that the balancing terms gives a consistent improvement. CIFAR-10 do not show much gain since all λ_S^{con} and λ_S^{cls} show similar values; in contrast, CIFAR-100 (super-class) and ImageNet-30 show large gain since they varies much.

Table 13: AUROC (%) values of our method without (w/o) and with (w/) balancing terms, under one-class (OC-) CIFAR-10, CIFAR-100 (super-class), and ImageNet-30. The values are averaged over classes, and bold denotes the best results. Balancing terms give consistent improvements.

	OC-CIFAR-10	OC-CIFAR-100	OC-ImageNet-30
CSI (w/o balancing)	94.28	89.00	91.04
CSI (w/ balancing)	94.31	89.55	91.63

G Combining multiple shifting transformations

We find that combining multiple shifting transformations: given two transformations \mathcal{S}_1 and \mathcal{S}_2 , use $\mathcal{S}_1 \times \mathcal{S}_2$ as the combined shifting transformation, can give further improvements. Table 14 shows that combining “Noise”, “Blur”, and “Perm” to “Rotate” gives additional gain. We remark that one can investigate the better combination; we choose rotation for our experiments due to its simplicity.

Table 14: AUROC (%) values of our method under various shifting transformations. Combining “Noise”, “Blur”, and “Perm” to “Rotate” gives additional gain.

	Noise	Blur	Perm	Rotate	Rotate+Noise	Rotate+Blur	Rotate+Perm
AUROC	89.29	89.15	90.68	94.31	94.65	94.66	94.60

H Discussion on the features of the contrastive score (6)

We find that the two features: a) the *cosine similarity* to the nearest training sample in the training set $\{x_m\}$, *i.e.*, $\max_m \text{sim}(z(x_m), z(x))$, and (b) the *feature norm* of the representation, *i.e.*, $\|z(x)\|$, are important features for detecting OOD samples under the SimCLR representation.

In this section, we first demonstrate the properties of the two features under vanilla SimCLR. While we use the vanilla SimCLR to validate they are general properties of SimCLR, we remark that our training scheme (see Section 2.2) further improves the discrimination power of the features. Next, we verify that cosine similarity and feature norm are *complementary*, that combining both features (*i.e.*, s_{con} (6)) give additional gain. For the latter one, we use our final training loss to match the reported values in prior experiments, but we note that the trend is consistent among the models.

First, we demonstrate the effect of cosine similarity for OOD detection. To this end, we train vanilla SimCLR using CIFAR-10 and CIFAR-100 and in- and out-of-distribution datasets. Since SimCLR attracts the same image with different augmentations, it learns to cluster similar images; hence, it shows good discrimination performance measured by linear evaluation [5]. Figure 3a presents the t-SNE [40] plot of the normalized features that each color denote different class. Even though SimCLR is trained in an unsupervised manner, the samples of the same classes are gathered.

Figure 3b and Figure 3c presents the histogram of the cosine similarities from the nearest training sample (*i.e.*, $\max_m \text{sim}(z(x_m), z(x))$), for training and test datasets, respectively. For the training set, we choose the second nearest sample since the nearest one is itself. One can see that training samples are concentrated, even though contrastive learning pushes the different samples. It complements the results of Figure 3a. For test sets, the in-distribution samples show a similar trend with the training samples. However, the OOD samples are farther from the training samples, which implies that the cosine similarity is an effective feature to detect OOD samples.

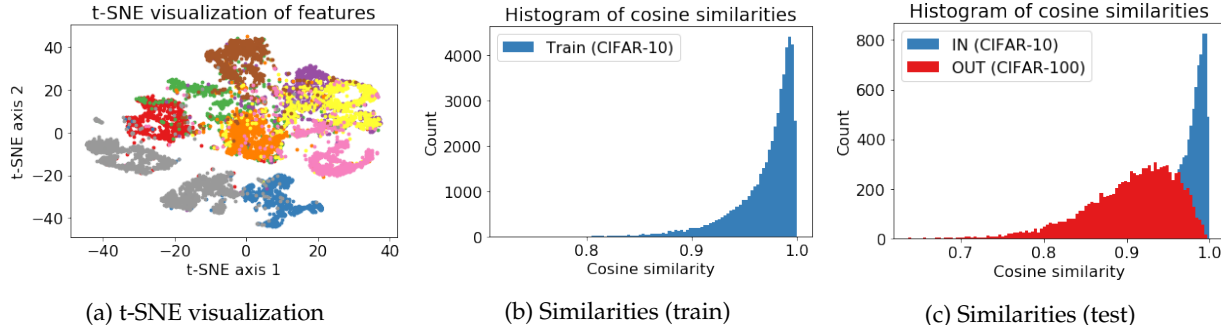


Figure 3: Plots for cosine similarity.

Second, we demonstrate that the feature norm is a discriminative feature for OOD detection. Following the prior setting, we use CIFAR-10 and CIFAR-100 for in- and out-of-distribution datasets, respectively. Figure 4a shows that the discriminative power of feature norm improves as the training epoch increases. We observe that this phenomenon consistently happens over models and settings; the contrastive loss makes the norm of in-distribution samples relatively larger than OOD samples. Figure 4b shows the norm of CIFAR-10 is indeed larger than CIFAR-100, under the final model.

This is somewhat unintuitive since the SimCLR uses the *normalized* features to compute the loss (1). To understand this phenomenon, we visualize the t-SNE [40] plot of the feature space in Figure 4c, randomly choosing 100 images from both datasets. We randomly augment each image for 100 times for better visualization. One can see that in-distribution samples tend to be spread out over the large sphere, while OOD samples are gathered near center.⁵ Also, note that the same image with different augmentations are highly clustered, while in-distribution samples are slightly more assembled.⁶

We suspect that increasing the norm may be an *easier* way to maximize cosine similarity between two vectors: instead of directly reducing the feature distance of two augmented samples, one can also increase the overall norm of the features to reduce the *relative* distance of two samples.

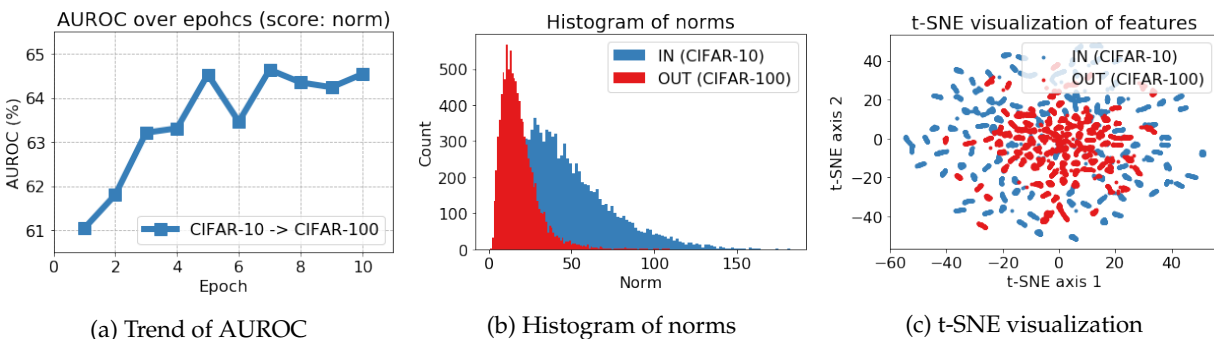


Figure 4: Plots for feature norm.

Finally, we verify that cosine similarity (sim-only) and feature norm (norm-only) are complementary: combining them (sim+norm) gives additional improvements. Here, we use the model trained by our final objective (5), and follow the inference scheme of the main experiments (see Table 7). Table 15 shows AUROC values under sim-only, norm-only, and sim+norm scores. Using only sim or norm already shows good results, but combining them shows the best results.

Table 15: AUROC (%) values for sim-only, norm-only, and sim+norm (*i.e.*, contrastive (6)) scores, under one-class (OC-) CIFAR-10, CIFAR-100 (super-class), and ImageNet-30. The values are averaged over classes. Using both sim and norm features shows the best results.

	OC-CIFAR-10	OC-CIFAR-100	OC-ImageNet-30
Sim-only	90.12	86.57	83.18
Norm-only	92.70	87.71	88.56
Sim+Norm	93.32	88.79	89.32

⁵t-SNE plot *does not* tell the true behavior of the original feature space, but it may give some intuition.

⁶We also try the local variance of the norm as a detection score. It also works well, but the norm is better.

I Rethinking OOD detection benchmarks

We find that resized LSUN and ImageNet [38], one of the most popular benchmark datasets for OOD detection, are visually far from in-distribution datasets (commonly, CIFAR [33]). Figure 5 shows that resized LSUN and ImageNet contain artificial noises, produced by broken image operations.⁷ It is problematic since one can detect such datasets with simple data statistics, without understanding semantics from neural networks. To progress OOD detection research one step further, one needs more *hard* or *semantic* OOD samples that cannot be easily detected by data statistics.

To verify this, we propose a simple detection score that measures the *input smoothness* of an image. Intuitively, noisy images would have a higher variation in input space than natural images. Formally, let $x^{(i,j)}$ be the i -th value of the vectorized image $x \in \mathbb{R}^{HWK}$. Here, we define the *neighborhood* \mathcal{N} as the set of spatially connected pairs of pixel indices. Then, the *total variation* distance is given by

$$\text{TV}(x) = \sum_{i,j \in \mathcal{N}} \|x^{(i)} - x^{(j)}\|_2^2. \quad (14)$$

Then, we define the *smoothness score* as the difference of total variation from the training samples:

$$s_{\text{smooth}}(x) := |\text{TV}(x) - \frac{1}{M} \sum_m \text{TV}(x_m)|. \quad (15)$$

Table 16 shows that this simple score detects current benchmark datasets surprisingly well.

To address this issue, we construct new benchmark datasets, using a fixed resize operation⁸, hence coined LSUN (FIX) and ImageNet (FIX). For LSUN (FIX), we randomly sample 1,000 images from every ten classes of the training set of LSUN. For ImageNet (FIX), we randomly sample 10,000 images from the entire training set of ImageNet-30, excluding “airliner”, “ambulance”, “parking-meter”, and “schooner” classes to avoid overlapping with CIFAR-10.⁹ Figure 6 shows that the new datasets are more visually realistic than the former ones (Figure 5). Also, Table 16 shows that the fixed datasets are not detected by the simple data statistics (15). We believe our newly produced datasets would be a stronger benchmark for hard or semantic OOD detection for future researches.

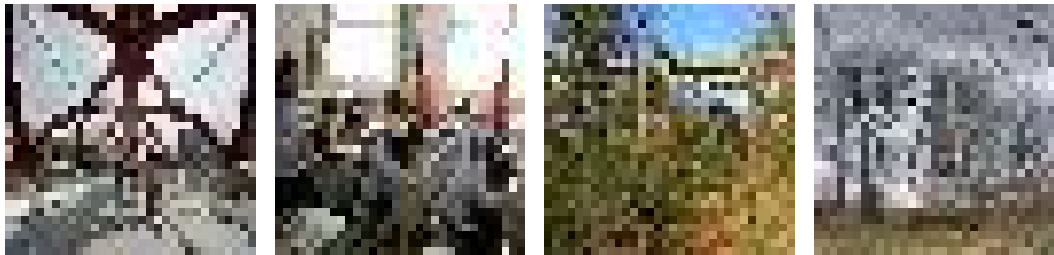


Figure 5: Current benchmark datasets: resized LSUN (left two) and ImageNet (right two).

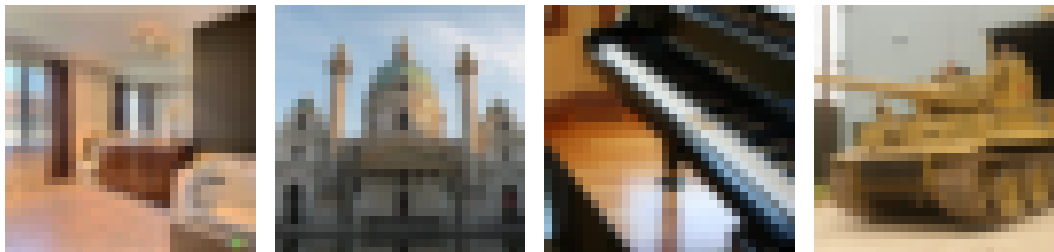


Figure 6: Proposed datasets: LSUN (FIX) (left two) and ImageNet (FIX) (right two).

⁷It is also reported in <https://twitter.com/jaakkolehtinen/status/1258102168176951299>.

⁸We use PyTorch `torchvision.transforms.Resize()` operation.

⁹We provide the datasets and data generation code in <https://github.com/alinlab/CSI>.

Table 16: AUROC (%) values using the smoothness score (15), under unlabeled CIFAR-10. Bold denotes the values over 80%, which implies the dataset is easily detected.

CIFAR10 →						
SVHN	LSUN	ImageNet	LSUN (FIX)	ImageNet (FIX)	CIFAR-100	Interp.
85.88	95.70	90.53	44.13	52.76	52.14	66.17

J Additional discussion on shifting transformation

As remarked in Section 3.2, the appropriate shifting transformation can be dependent on the dataset. It is crucial for real-world scenarios since many practical applications deal with non-natural images, *e.g.*, manufacturing - steel¹⁰ or textile¹¹ for instance, or aerial [63] images. For such datasets, one should *not* use rotation as a shifting transformation. We present OOD detection results using Steel and ImageNet-30 as in- and out-of-distribution datasets, respectively. Table 17 shows similar results with the one in Section 3.2: shifting rotation degrades the performance. Investigating new transformations considering the characteristics of the datasets would be an interesting future direction.

Table 17: AUROC (%) on Steel dataset, where ImageNet-30 is used for OOD.

SimCLR	CSI (Rotation)
74.0	36.0

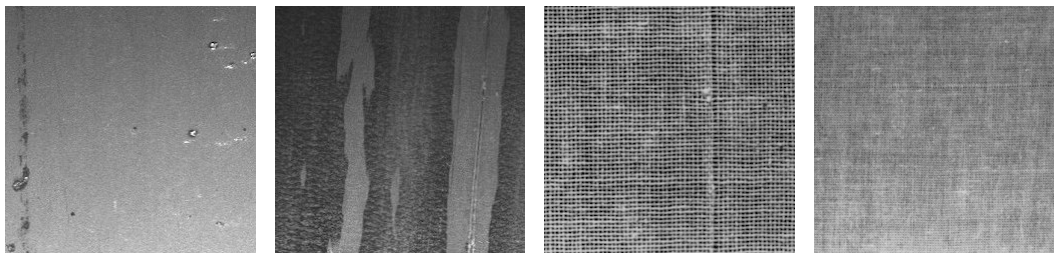


Figure 7: Examples of steel (left two) and textile (right two) images.



Figure 8: Examples of aerial images.

¹⁰<https://www.kaggle.com/c/severstal-steel-defect-detection>

¹¹<https://lmb.informatik.uni-freiburg.de/resources/datasets/tilda.en.html>